ELSEVIER

Analytica Chimica Acta 380 (1999) 47–54

ANALYTICA CHIMICA ACTA

Inverse derivative chronopotentiometry/quartz crystal microgravimetry of solid conducting salt films

K.M. Scaboo, W.H. Grover, J.Q. Chambers*

Chemistry Department, University of Tennessee, Knoxville, TN, 37996, USA

Received 10 July 1998; received in revised form 6 September 1998; accepted 10 September 1998

Abstract

An instrument, built in-house, for the purpose of making derivative chronopotentiometric and quartz crystal microgravimetric measurements is described. The spreadsheet-based software allows for presentation of the raw or derivative data of both the chronopotentiometric and gravimetric measurements in either the time or potential domain. The system was used to study the nucleation-controlled growth of the phase transition associated with the TCNQ(0/−1) couple isolated from a thin film of the conducting salt 9-aminoacridinium tetracyanoquinodimethane. The dt/dE–E curves for a nucleation process are presented along with the Hillman–Bruckenstein analysis of the corresponding mass changes of the film.

Keywords: Conducting organic salts; Tetracyanoquinodimethane; Inverse derivative chronopotentiometry; Nucleation; Quartz crystal microbalance

1. Introduction

In the last ten years there has been an increased interest in derivative chronopotentiometric measurements due to the high sensitivity that can be achieved for both surface confined and diffusional electroactive species. One of the most convenient formats for presentation of this type of data is the dt/dE vs. potential (E) curve that is the basis for the well-known potentiometric stripping analysis (PSA). This method has been used in studies of oligonucleotides, proteins, and for the determination of trace metal species [1–6]. Recently, the equations describing the dt/dE–E curves for a reversible diffusional couple subjected to current reversal chronopotentiometry have been presented and verified with experiment [7]. Both methods report a substantial gain in sensitivity over conventional cyclic voltammetry.

When presented in the potential domain, the dt/dE curves bear close resemblance to voltammetric style peaks, allowing for convenient measurement of species concentration and determination of reversibility. The derivative nature of the data has allowed for determination of the transition time (τ) from the peak height without the errors due to double layer charging that plagued the graphical measurement of τ using the traditional E–t curves [8]. The resemblance to voltammetric I–E curves was recognized by electroanalytical chemists long before it was possible to manipulate spreadsheet data with a few key strokes [8–10]. Advances in commercial software make it very easy

*Corresponding author. Tel.: +1-423-974-3141; fax: +1-423-974-3454.

0003-2670/99/$ – see front matter
PII: S0003-2670(98)00647-3

to collect and manipulate the experimental data to obtain numerous forms of presentation for a single measurement.

The intuitive nature of the instrumentation associated with chronopotentiometry makes this technique very conducive to coupling with ancillary analytical methods. Here we present a simple setup, built in-house, for the purpose of making derivative chronopotentiometric measurements. The software allows for presentation of the chronopotentiometric data in either the traditional E vs. t form or in any of the derivative forms (dE/dt vs. t or E, or dt/dE vs. t or E). We have incorporated a quartz crystal microbalance (QCM) into the instrumentation in order to study the TCNQ(0/−1) couple that was isolated from a mechanically applied polycrystalline film of the conducting salt 9-aminoacridinium tetracyanoquinodimethane. This system provides an example of a relatively complex surface reaction involving nucleation-controlled growth [11–13] of the solid-state phase transition accompanied by electrolyte ion migration into and out of the film to maintain charge balance [14]. The accompanying mass data can also be differentiated and presented in either the time or potential domain. This, along with the advantage of the constant charge flux associated with chronopotentiometric measurements, made for easy analysis of the mass changes using the Hillman and Bruckenstein method [15,16]. This method allows for deconvolution of the contributions from ionic and neutral species to the total mass change that occurs along with the Faradaic phase transition.

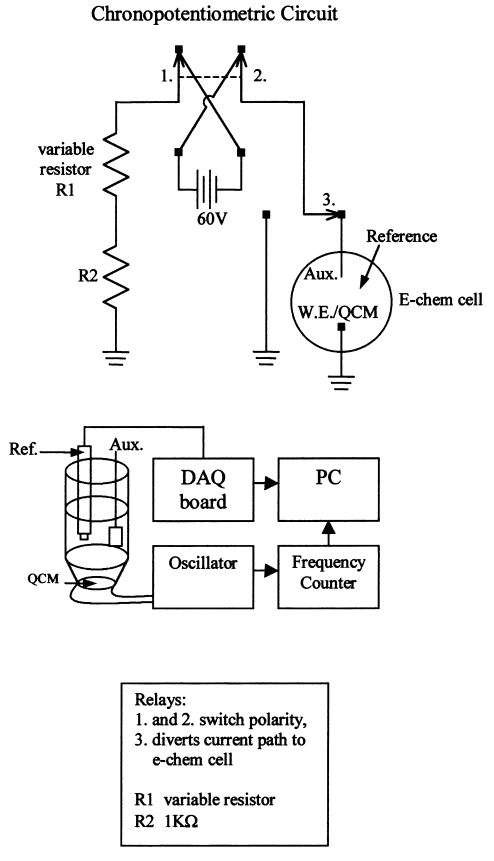

Fig. 1. Circuit diagram for the instrument used to make the chronopotentiometric and gravimetric measurements.

2. Experimental

2.1. Data acquisition and analysis

The apparatus for the acquisition of the chronopotentiometric measurements was constructed in-house and controlled and monitored using a PC equipped with a National Instruments Data Acquisition Board Model no. AT-MIO-16DL-9 and LabVIEW version 4.1 software. Two Eveready 30 V batteries placed in series were used as the current source and the polarity and path of the current were controlled using Clarion model LCC110 SPDT relays as shown in the circuit diagram of Fig. 1. The magnitude of the current was controlled by changing the value of resistor R1 in the figure and gave a usable current range of about 2–40 μA. The use of a grounded working electrode and a direct current power supply allowed for low system noise, which is imperative when using a derivative method of analysis and a requirement for the conventional QCM oscillator circuitry.

The quartz crystals were driven to oscillation using a 12 V DC power supply and monitored using a conventional oscillator circuit. A Keithley model 775 A frequency counter was used which communicated with the PC using a National Instruments AT-GPIB-TNT plug and play card. The latter was also controlled by the LabVIEW software.

The data analysis routine was incorporated into the same program as the data acquisition allowing for immediate access to the desired data presentation. The analysis consisted of a numerical derivation of the

potential data with respect to time (dE/dt) and then an inversion of the resulting data set to obtain dt/dE. These data could then be presented with respect to either time or the corresponding potentials. Even with the low system noise, it was still necessary to perform some simple smoothing functions on the data to extract the desired information in usable form. The program allows for smoothing of the data at any point in the analysis using a Savitzky–Golay quadratic–cubic regression routine or a mean filter routine [17,18]. The data file could also be written to a text file at any point for the desired presentation.

2.2. Electrochemical

The instrument was first tested on a well-documented diffusional couple in order to compare the results to those presented by Bi and Yu [7]. A 1 mM solution of potassium hexacyanoferrate(III) was measured using a glassy carbon working electrode (A=0.0707 cm^2), a platinum coil auxiliary electrode, and a saturated calomel reference electrode (SCE). Driving currents in the range 9–40 μA were employed. The glassy carbon working electrode was polished extensively using 0.3 μM alumina and a rotary polishing pad. The results correlated well with those of Bi and Yu.

The 9-aminoacridinium tetracyanoquinodimethane was obtained from a previous study [14]. The 5 MHz AT-cut quartz crystals were supplied by ICM corporation of Oklahoma City. The crystals had 6.8 mm Au working electrodes vapor deposited on both sides (A=0.363 cm^2). The electrochemical cell was constructed by attaching the crystals to a glass tube with an end diameter slightly larger than the electrode surface using Devcon 5 min epoxy cement. A platinum coil and a SCE were used as the counter and reference electrodes, respectively. The conducting salt film was mechanically applied to the gold electrode using a cotton swab so that the entire surface was covered. A 1 M solution of potassium acetate ($KC_2H_3O_2$) was employed as the supporting electrolyte. The $KC_2H_3O_2$ was obtained from Mallinkrodt Specialty Chemical and was used as received. The film was electrochemically activated by potential cycling from 600 to −100 mV and back to 400 mV at a sweep rate of 10 mV/s using a Cypress Systems model CS-2Ra electrochemical analyzer.

3. Results and discussion

After initial activation of the film by oxidation at 600 mV, as has been well documented in previous reports [11,14], a persistent irreversible couple is apparent in the cyclic voltammograms (CVs). This couple corresponds to the reduction and subsequent oxidation of the TCNQ sites:

$$\mathrm{TCNQ} + \mathrm{K}^+_{\mathrm{aq}} + \mathrm{e}^- \Leftrightarrow \mathrm{TCNQ}^-, \mathrm{K}^+. \quad (1)$$

A CV showing the activation process and the resulting TCNQ couple is shown in Fig. 2. This is a typical result for these films, showing the large peak separation and narrow peak widths associated with conducting salt voltammetry. Voltammetric and chronoamperometric evidence [11,12] points to the involvement of nucleation phenomena in the phase transition and it has been shown using a quartz crystal microbalance that the phase transition is accompanied by potassium ion migration into the film during the reduction and out of the film during the subsequent oxidation [11]. Thus these films are representative of a rather complex system where both nucleation-driven electron transfer kinetics and diffusional behavior contribute to the rate of electron transfer.

Both the potentiometric measurements and the accompanying quartz crystal frequency responses were recorded simultaneously and the results were worked up using the analysis program outlined above. An example of the raw data output for these films is

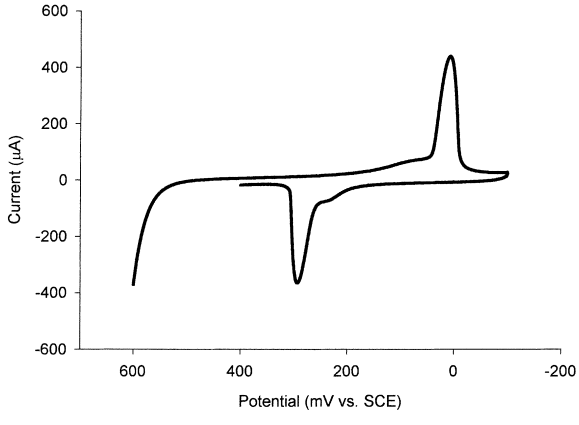

Fig. 2. Cyclic voltammogram describing the activation process. The scan direction is initially negative at a scan rate of 10 mV/s.

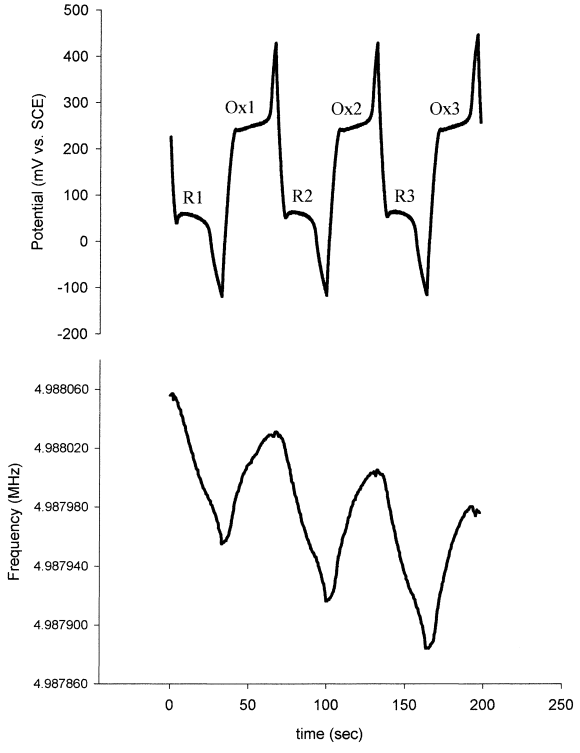

Fig. 3. Raw chronopotentiometric (top) and quartz crystal frequency (bottom) output for the 9AA$(TCNQ)_2$ film shown in Fig. 2. Current=26 μA.

shown in Fig. 3. This data set was obtained using a current of 26 μA after repetitive redox cycling had already occurred to give a stable reproducible cyclic voltammogram. Similar results were obtained for 9 and 40 μA driving currents. It is important to note the potential maxima or minima that are apparent in both the reductive and oxidative plateaus. This is a well-documented feature characteristic of nucleation phenomena [19–25]. As can be seen, the frequency data are consistent with a mass increase during the reduction and a corresponding decrease in mass during the oxidation. It should be noted that the time frame for this experiment is slow relative to the ion exchange phenomena known to occur during redox transformation [14].

3.1. Potentiometric data

The dt/dE vs. E response for a simple reversible, surface confined redox couple was first presented by Jin and Wang [26] and is well documented. The result is a voltammetric-style peak where the peak potential is independent of the surface coverage and the peak height is a function of the transition time (τ) and thus the surface coverage. The peak width at half height should correspond to 90.6 mV/n. To our knowledge, however, the representative dt/dE–E curve for a process involving nucleation kinetics has not been presented and as will be seen, is not as simple as the above case.

Fig. 4 shows the potentiometric raw data along with the various derivative presentations corresponding to the reduction (R2 of Fig. 3) of the TCNQ sites within the polycrystalline film. In Fig. 4(a), the potential of the system initially swings sharply in the negative direction until it reaches a minimum that presumably corresponds to the energy of initial nucleation center reduction. After the nucleation centers have been reduced, the completion of the phase transition is more energetically favorable and the potential shifts back in the positive direction until the reduction is complete. This behavior results in a derivative curve that has two points where dE/dt is equal to zero. The first value of zero occurs at the peak negative potential and then dE/dt is positive as the potential swings back to the potential maxima of the phase transition where the second zero value of dE/dt occurs. These features are seen in the dE/dt–time curve of Fig. 4(b).

When the time derivative data are presented vs. the corresponding potentials, as in Fig. 4(c), the energy overlap becomes even more apparent in the form of a potential loop that crosses the dE/dt value of zero twice. When the inverse of the derivative data is taken to obtain dt/dE, which is plotted vs. potential in Fig. 4(d), discontinuity in the curve is observed at the points where dE/dt equals zero. For well-behaved surface redox transitions [26], or diffusion-controlled electrode reactions [7], this data presentation produces a well-defined peak comparable to voltammetry. Thus this discontinuity is indicative of a nucleation phenomenon where the overpotential is decreased once the nucleation and growth process commences. The voltage difference between the points of discontinuity is the magnitude of the potential overlap occurring during the course of the reduction.

The data for the subsequent oxidation (Ox 1 of Fig. 3) of the couple are presented in the same manner as above in Fig. 5. There was one consistent, signifi-

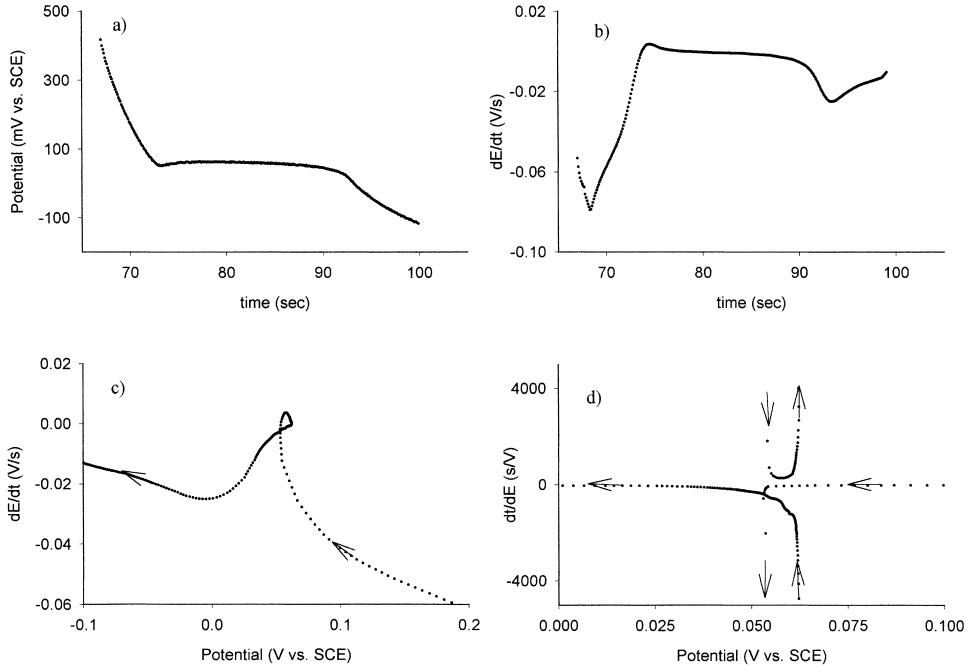

Fig. 4. Raw (a) and derivative (b)–(d) responses for the second reductive cycle (R2 of Fig. 3). The arrows in the potential domain presentations (c), (d) show the direction of the potential response.

cant difference seen between the reduction and oxidation processes involving the magnitude of the voltage overlap occurring during the phase transition: in virtually all of the films studied, the voltage overlap seen in the d*E*/d*t*–E curves for the oxidation was of a much smaller magnitude than that for the reduction process. In the film shown in Fig. 5, the magnitude of the overlap approached the lower limit of voltage resolution achieved during the experiment. This difference suggests that the cathodic process has a significantly higher potential barrier to overcome for the initial nucleation center phase change.

Another interesting point demonstrated in Fig. 5(d) is the instability of the potential during the oxidative phase transition which resulted in multiple peaks occurring within a relatively small voltage range. This was also seen in the reduction process, though to a lesser extent. This behavior was seen repeatedly in experiments involving the 9-AA(TCNQ)$_2$ conducting salt. We are uncertain whether this behavior corresponds to multiple nucleation processes or small variations in the driving current. Similar behavior has been seen in previous chronoamperometric and voltammetric experiments on both polycrystalline films and single crystal conducting salt electrodes [11,13,27]. However, for the classical chronoamperometric measurements, only two distinct processes could be resolved. More processes were hinted at within the curve, but deconvolution was unsuccessful. In the case of the voltammetric experiments, similar results to that seen in Fig. 5(d) were seen at sweep rates $\leq$250 μV/s. Thus there is precedence for the idea of multiple nucleation processes occurring within the film but the origin of the possible multiplicity remains elusive.

3.2. Frequency data

The frequency data obtained concomitant with the potentiometric data provided greater insight into the nature of the mass changes associated with the phase transitions of the polycrystalline film. Earlier EQCM studies of these films [14] utilized the Hillman and Bruckenstein analysis [15,16] to reveal that substantial neutral species transfer occurred at the electrode interface during redox transformations. This method of

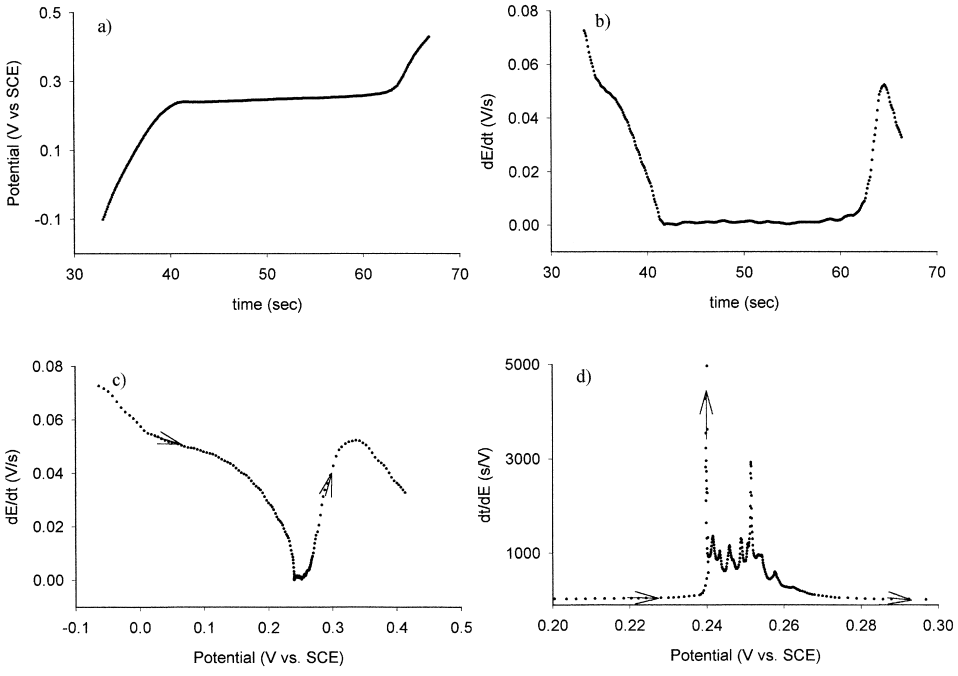

Fig. 5. Raw (a) and derivative (b)–(d) responses for the first oxidative cycle (Ox1 of Fig. 3). The arrows in the potential domain presentations (c), (d) show the direction of the potential response.

analysis allows for both identification of the major ion contributing to charge transfer and the resolution of any mass changes due to transfer of neutral species. The data obtained in this study were treated using this same approach.

The total mass change (ΔM) is a linear combination of the mass change attributed to the charged species and that due to any neutral species transferred:

$$\Delta M = \Phi - Q(m_j/zF), \tag{2}$$

where Φ is the contribution of any neutral species and the term $Q(m_j/zF)$ accounts for the contribution of the major charged species with charge z and molar mass m_j. If the mass change is due only to permselective ion exchange, then by definition, Φ=0 and a plot of ΔM vs. Q would give a linear response with a slope of m_j/zF. For the case where both charged and neutral species are exchanged, the mass of the major ionic species being transferred can be determined by selecting the mass that minimizes the Φ term in Eq. (1) for a given set of experimental data. Once this has been accomplished, Φ can then be used to give information on the dynamics of the neutral species exchange.

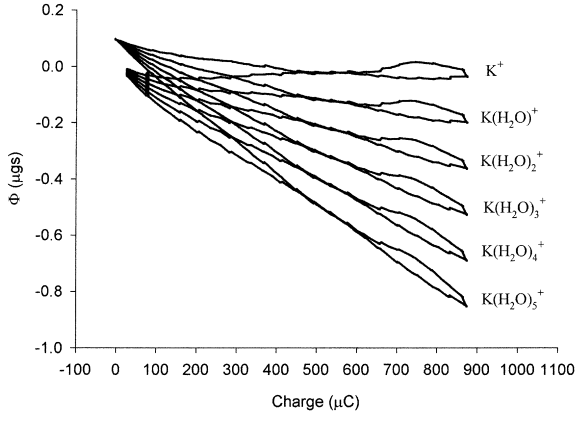

Fig. 6. The Φ minimization routine of the gravimetric data using the Hillman–Bruckenstein analysis for the first complete redox cycle (R1 and Ox1 of Fig. 3). Masses were chosen corresponding to different degrees of hydration of the potassium ion.

Fig. 6 demonstrates the minimization routine used to identify the mass of the major ion involved in the mass transfer for the first redox couple. Mass values were selected corresponding to different degrees of hydration of the potassium ion. It can be seen from the

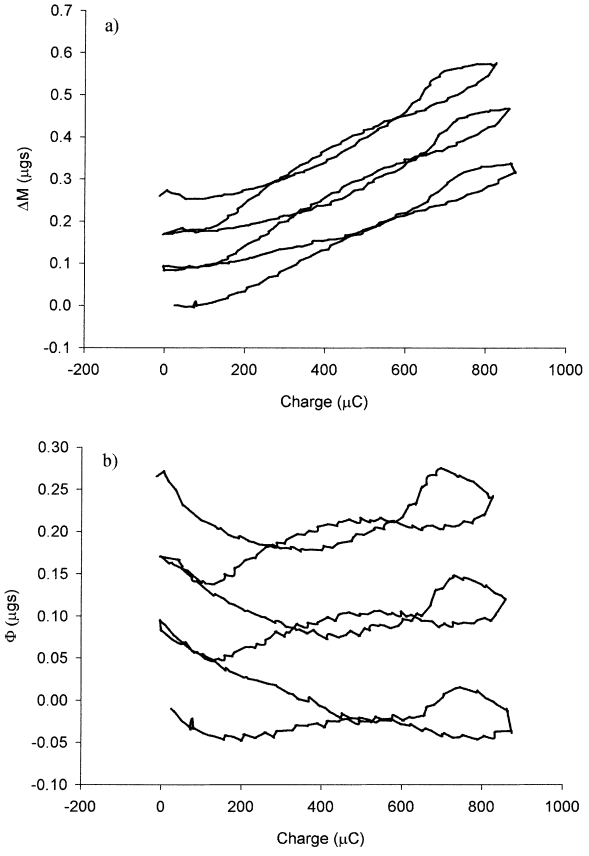

Fig. 7. (a) Total mass change vs. charge (Q) for all three redox cycles of Fig. 3. (b) Φ vs. charge (Q) for all three redox cycles using the mass of 39 g/mol (K^+) for the major charge-carrying species.

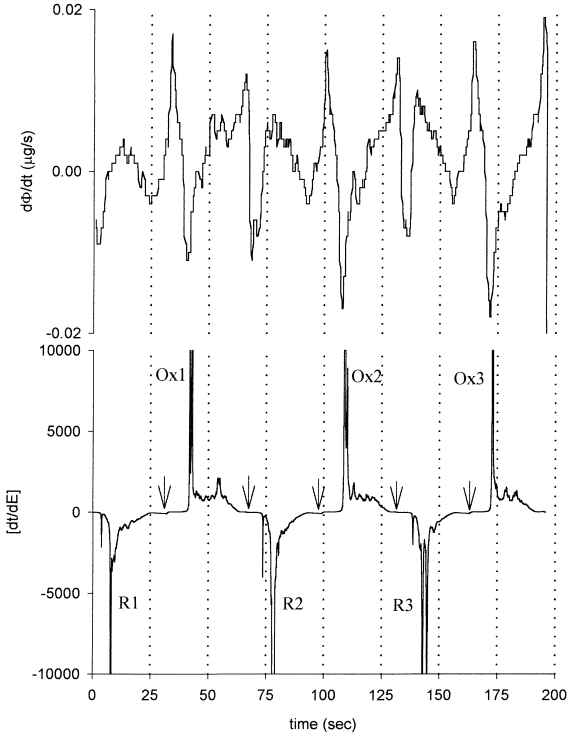

Fig. 8. dΦ/dt (top) and (dt/dE) (bottom) vs. time for all three cycles of Fig. 3. Cathodic (dt/dE) responses are given a negative value. Arrows indicate the times of current reversal.

figure that Φ is minimized when the ion mass selected is equal to that of a bare potassium ion. Equivalent masses calculated from the frequency changes at the switching times using the Sauerbrey equation were 40, 38 and 30 ($s_{\text{pooled}}=\pm 9$) at I=9, 26 and 40 μA, respectively.

Fig. 7 shows ΔM and Φ as a function of charge for all three of the redox cycles. The increasing positive deviation in the Φ plots of each subsequent cycle from zero indicates that the film is becoming increasingly hydrated throughout the course of the experiment and is consistent with earlier results [14].

In Fig. 8, the absolute values of dt/dE and dΦ/dt are plotted vs. time for all three redox cycles. For presentation and convention sake, the (dt/dE) data for the reduction process are given a negative sign. This convenient plot allows one to see that the rate of *apparent* neutral species transfer is of the greatest magnitude at times just before the onset of the redox transformation. This is especially true for the oxidation process where the rate of transfer of the neutral species declines sharply during the actual Faradaic process. This response is not completely understood, but may be related to the large pseudocapacitance that has been demonstrated in the past [11] to be present between the potentials of the anodic and cathodic peaks for the TCNQ(0/−1) couple. This pseudocapacitance can be seen in the voltammetric response of Fig. 2 in the form of prewaves preceding the peak voltammograms. This signal has been shown to be Faradaic in nature, thus some type of mass change would be expected in order to achieve charge balance.

It should be noted that galvanostatic techniques are especially suited to this type of analysis due to the fact that the charge flux is constant throughout the experiment. While similar information is available from both

voltammetric and chronopotentiometric EQCM on conducting salts [14,28], the latter technique provides a data set where Q is a linear function of time without the need for any normalization. Thus for the ideal case where only the charge-carrying species contributes to the mass change, the frequency data should scale in a linear fashion with time, giving a sawtooth response. This allows for immediate visual qualitative assessment of the system; any contribution to the mass change by a neutral species will result in a deviation from linearity in the raw data set.

4. Conclusions

Derivative chronopotentiometric techniques offer the advantage of simple, inexpensive instrumentation coupled with excellent sensitivity and very high resolution. The system presented here displays all of the above attributes and demonstrates the ease to which this type of setup can be coupled to other suitable instrumentation such as a quartz crystal microbalance to give an informative perspective on a given phase transition. A real advantage is seen in using a software-based analysis routine that allows for presentation of the raw potentiometric and frequency data or both of the derivative forms vs. either time or potential. The application of this analysis to a nucleation-driven redox reaction revealed a discontinuous dt/dE–E curve due to the potential overlap that is inherent to these types of processes. The QCM data obtained during the chronopotentiometric experiment were readily analyzed using the Hillman–Bruckenstein analysis due to the fact that the charge flux is constant throughout the course of the experiment.

Acknowledgements

This research was supported by a grant from the National Science Foundation (CHE-9616994) and the University of Tennessee. Dr. Vilmos Kertesz and Dr. Tracy Staller are thanked for their helpful comments.

References

[1] H. Eskilsson, C. Haraldsson, Anal. Chim. Acta 175 (1985) 79.
[2] E. Palecek, M. Tomschik, V. Stankova, L. Havran, Electroanalysis 9 (1997) 990.
[3] M. Fojta, L. Havran, E. Palecek, Electroanalysis 9 (1997) 1033.
[4] J. Wang, G. Rivas, D. Luo, X. Cia, F.S. Valera, N. Dontha, Anal. Chem. 68 (1996) 4365.
[5] D. Jagner, Y. Wang, Electroanalysis 7 (1995) 614.
[6] M.J. Honeychurch, M.J. Ridd, Electroanalysis 9 (1997) 261.
[7] S. Bi, J.J. Yu, J. Electroanal. Chem. 405 (1996) 51.
[8] A.J. Bard, L.R. Faulkner, Electrochemical Methods, Wiley, New York, 1980, p. 269.
[9] W.H. Reinmuth, Anal. Chem. 32 (1960) 1509.
[10] C.N. Reilley, G.W. Everett, R.H. Johns, Anal. Chem. 27 (1955) 483.
[11] J.Q. Chambers, K. Scaboo, C.D. Evans, J. Electrochem. Soc. 143 (1996) 3039.
[12] A.M. Bond, S. Fletcher, R. Marken, S.J. Shaw, P.G. Symons, J. Chem. Soc., Faraday Trans. 92 (1996) 3925.
[13] K.M. Scaboo, J.Q. Chambers, Electrochim. Acta 43 (1998) 3257.
[14] C.D. Evans, J.Q. Chambers, Chem. Mater. 6 (1994) 454.
[15] A.R. Hillman, M.J. Swann, S.J. Bruckenstein, J. Phys. Chem. 95 (1991) 3271.
[16] A.R. Hillman, D.C. Loveday, S.J. Bruckenstein, J. Electroanal. Chem. 300 (1991) 67.
[17] D. Gilmore, Savitzky–Golay Quadratic–Cubic and Quartic–Quintic Smoothing Function, ftp://ftp.pica.army.mil/pub/labview/vi/lv3.0/s_g_smth.llb (accessed April 1998).
[18] U. Frenz, Moving Average Filter, ftp://ftp.pica.army.mil/pub/labview/vi/lv4/meanfilt.vi (accessed April 1998).
[19] A. Dobreva, Cryst. Res. Technol. 25 (1990) 927.
[20] S. Fletcher, A. Smith, Can. J. Chem. 56 (1978) 908.
[21] J.A. Harrison, W.J. Lorenz, J. Electroanal. Chem. 76 (1977) 375.
[22] G.J. Hills, L.M. Peter, B.R. Scharifker, M.I. daSilva-Pereira, J. Electroanal. Chem. 124 (1981) 247.
[23] A. Milchev, M.I. Montenegro, J. Electroanal. Chem. 333 (1992) 93.
[24] M. Peykova, E. Michailova, D. Stoychev, A. Milchev, Electrochim. Acta 40 (1995) 2595.
[25] Z.J. Suturovic, N.J. Marjanovic, Electroanalysis 9 (1997) 572.
[26] W. Jin, J.J. Wang, J. Electroanal. Chem. 306 (1991) 31.
[27] J.Q. Chambers, D.C. Green, F.B. Kaufman, E.M. Engler, B.A. Scott, R.R. Schumaker, Anal. Chem. 49 (1977) 802.
[28] S.J. Shaw, F. Marken, A.M. Bond, Electroanalysis 8 (1996) 732.